EFFECT OF *IN VITRO* MAGNETIC FLUID HYPERTHERMIA USING CITRATE COATED COBALT FERRITE NANOPARTICLES ON TUMOR CELL DEATH

HEBA KAHIL[*#], H.M. EL_SAYED[**], E.M. ELSAYED[*], A.M. SALLAM[*], MONA TALAAT[*], A.A. SATTAR[**]

[*] Biophysics Laboratory, Physics Department, Faculty of Science, Ain Shams University, Cairo, Egypt, [#]hebakahil@gmail.com
[**] Magnetism Laboratory, Physics Department, Faculty of Science, Ain Shams University, Cairo, Egypt

Abstract. Magnetic fluid hyperthermia (MFH) has been proved to be a promising modality for the treatment of tumors. The specific absorption rate (SAR) is thoroughly investigated in water based colloids; whereas scarce data is available on the SAR values inside biological media. Elevated salt content, presence of proteins and cellular structures are assumed to affect SAR values; a fact that should be considered when determining therapeutic doses. This study presents the preparation of cobalt ferrite magnetic nanoparticles (MNPs) using coprecipitation method with particle size of 13.56 ($\sigma = 0.14$) nm and sodium citrate used as coating. The obtained SAR value was 82.6 W/g at a magnetic field intensity of 9.4 kA/m and frequency of 198 kHz in water based fluid and decreased to 23.3 W/g in saline based solution and to a slightly higher value of 29.8 W/g in Ehrlich ascite carcinoma suspension. The effect of MNPs concentration and the therapeutic temperature on the Ehrlich ascite carcinoma cell viability were also studied. This revealed that an optimum concentration of 8 mg/mL and a temperature of 57 °C led to complete cell death after 30 minutes of exposure at the previously mentioned field and frequency. The results showed that cobalt ferrite can be regarded as a promising candidate for MFH.

Key words: Magnetic nanoparticles (MNPs), cobalt ferrite, SAR, *in vitro* magnetic fluid hyperthermia (MFH).

INTRODUCTION

Cancer is currently one of the leading killer diseases. Annually, about 7 million people die of cancer which is expected to reach 17 million deaths in 2030 [17]. For this reason cancer therapy has been a challenge for decades. A convenient therapy in many cases is hyperthermia; which is regarded as a therapeutic procedure involving the raising of tissue temperature above normal physiological

conditions. Magnetic fluid hyperthermia – first proposed by Gilchrist *et al.* in 1957 – has shown to be a promising therapeutic technique [11]. MFH is based on the internalization of MNPs into tumor site and subsequently exposing the patient to an alternating magnetic field (AMF). MNPs absorb the energy from the AMF and generate heat that is transferred by conduction to the adjacent tumor cells. Regarding the rise in temperature, thermotherapy is divided into hyperthermia and thermoablation [14]. Hyperthermia involves heating certain organs or tissues to temperatures between 41 °C and 46 °C. This moderate rise in temperature may alter the function of many structural and enzymatic proteins leading to cellular degradation followed by signaling of apoptosis. However, moderate hyperthermia sensitizes the tumor cells for radiation [13, 33] and chemotherapeutic drugs [42] therefore, it is utilized in treatments that may last for hours of combined therapy. On the other hand, thermoablation involves heating certain organs or tissues to temperatures above 46 °C and thus causes direct cytotoxic effects leading to certain cell death even in case of acute treatments lasting for few minutes [6]. This therapeutic pathway ultimately results in tissue necrosis, coagulation or carbonization [22] and may also affect normal cells. Internalization of MNPs is assumed to allow better control of thermal energy inside the tumor. Cobalt ferrite ($CoFe_2O_4$) which has a spinel structure is selected as the magnetic species. $CoFe_2O_4$ has been proposed for a variety of biomedical applications [3, 4] including MFH in an attempt to find new candidates for the well-known iron oxide MNPs. It has the advantages of chemical stability and large anisotropy [1]. The large anisotropy allows for the production of particles with high SAR values a yet small particle size.
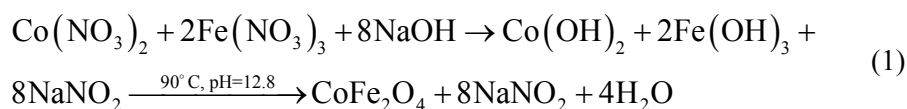
The heating capability of the particles is quantified in terms of the specific absorption rate (SAR) ; thermal energy dissipated by MNPs per unit time and mass [16] . SAR values are frequency and field dependent. The applied frequency throughout this study was 198 kHz. The FDA proposed a limit for the product of ($f \cdot H$) of (3.83×10^9 kA/ms) at 200 kHz [19] and a more relaxed criterion was proposed by Herget ($H \cdot f < 5 \times 10^9$) [12].

It is a well-established fact that the effect of actual physiological conditions (pH = 7 and 0.9% salinity) [5] on SAR values determines the biocompatibility of the cobalt ferrite particles and the validity of their use in hyperthermia. Nevertheless, scarce data is available on the impact of actual physiological conditions on the SAR values compared to their counterparts measured in water. For this reason, the aim of the study is to investigate the variation of the calculated SAR values of the cobalt ferrite sample in water and in saline based fluids. To complete the analysis SAR was computed in an Ehrlich ascite cell suspension for the purpose of simulating actual physiological conditions. Ehrlich ascite cell suspension contains in addition to the NaCl content, other minerals, serum proteins (opsions) and cells with charged membranes. All the mentioned parameters are assumed to further affect the stability of the MNPs in solution.

MATERIALS AND METHODS

PREPARATION OF CoFe₂O₄ BASED MF

Coprecipitation, a wet method that produces fine particles, has been utilized by several authors [25, 34] and was used in this study for the synthesis of cobalt ferrite MNPs [31]. Sodium citrate was selected as a surfactant to enhance the surface charge of the MNPs for the purpose of forming a stable colloid [9, 26]. Citrate coated cobalt ferrite MNPs are considered as a biocompatible base for magnetic fluid (MF) [21]. All chemicals employed are analytical grade and used without further purification. Iron and Cobalt nitrates at the molar ratio 2:1 were separately dissolved in distilled water then added under continuous stirring. 8 moles of NaOH were added dropwise from a burette to the reaction vessel that contained the nitrate precursors until the neutral pH was reached and then excess of NaOH was readily added until the final pH reached 12.8 then heating started. The reaction is described by

$$Co(NO_3)_2 + 2Fe(NO_3)_3 + 8NaOH \rightarrow Co(OH)_2 + 2Fe(OH)_3 +$$
$$8NaNO_2 \xrightarrow{90°C, pH=12.8} CoFe_2O_4 + 8NaNO_2 + 4H_2O$$

$$(1)$$

The black magnetic phase (formed after 90 min at 90 °C) was then washed several times with distilled water till pH dropped to 7. This uncoated sample is indexed as (CF). To form citrate coated MNPs (CFC), the sample (CF) was dissolved in water and ultrasonically agitated for 60 minutes then stirred at 80 °C for two hours in a saturated solution of sodium citrate, and finally washed several times with distilled water.

STRUCTURAL ANALYSIS

The structure of the prepared samples was determined using X-ray powder diffraction (XRD), Transmission electron microscopy (TEM), Electron diffraction, Fourier transform infrared (FTIR) spectra. Particle stability was determined *via* measuring the zeta potential and the hydrodynamic volume. X-ray powder diffraction patterns of the samples were collected on a Philips diffractometer (X'pert MPD) with Cu-Kα radiation. The diffracted intensities were collected in step-scan mode (step size 2θ = 0.02°; counting time 2 s) in the angular range 2θ = 20–80 °. To correct instrumental broadening LaB6 standard was used. The sample structure and microstructure were refined applying Rietveld profile method, using MAUD program (L. Lutterotti, Maud 2.33) [23]. High resolution transmission electron microscope (HR-TEM, Tecnai G20, FEI, Netherlands) was used for imaging particle morphology, crystal planes and size calculation. Two

different modes of imaging were employed; the bright field at electron accelerating voltage 200 kV using lanthanum hexaboride (LaB6) electron source gun and the diffraction pattern imaging. Eagle CCD camera with (4k · 4k) image resolution was used to acquire and collect transmitted electron images. Fourier transform infrared (FTIR) spectra were recorded by Nicolet 6700 at 4 cm^{-1} resolution. The FTIR spectra were measured in the 400–4000 cm^{-1} region with samples dispersed in KBr pellets. The zeta sizer (Malvern, UK) nano series (Nano ZS) was used to determine the zeta potential based on electrophoretic mobility as well as the hydrodynamic volume based on dynamic light scattering.

SAR MEASUREMENTS

For the assessment of SAR, a high power induction heater (DW-VHF 10 kW, China) is required as the particles are generally used in low concentrations (few mgs per mL) and the solvent is water with high specific heat. SAR values of the samples were determined by the non-adiabatic time-dependent calorimetric measurements [24] (setup shown in Fig. 1). The induction heater used here allows a single frequency measurement (198 kHz). This frequency is one of the available frequencies in the induction heater that is close to the resonant frequency of the samples. It is worth mentioning that the frequency response of the sample to the AMF in the frequency range between (120 and 230 kHz) was performed in our laboratory and a resonance was obtained around 180 kHz. In all experiments, a constant volume of the colloid was contained in a plastic vial (polyvinyl chloride (PVC)) that was inserted in a Styrofoam jacket. The temperature was measured using an alcohol thermometer [40]. In case of *in vitro* SAR measurement, cells were incubated with sample CFC for 30 minutes at 37 °C in the exposure vial. The alcohol thermometer was inserted in the sample for 1 minute prior to switching on the field. SAR was determined from equation (2) [30],

$$SAR = \frac{\sum_i c_i m_i}{m_{CoFe_2O_4}} \frac{\Delta T}{\Delta t} \qquad (2)$$

where c_i and m_i are the individual specific heat and mass of water and the PVC vial. The heat capacity of cobalt ferrite is ignored due to its low concentration. The specific heat of water and PVC are 4.18, and 0.9 Jg^{-1} K^{-1} respectively and their masses are 3 and 2.16 grams respectively. $\Delta T/\Delta t$ is the initial slope of the time-dependent temperature curve and $m_{CoFe_2O_4}$ is the mass of CoFe$_2$O$_4$ in the sample in grams.
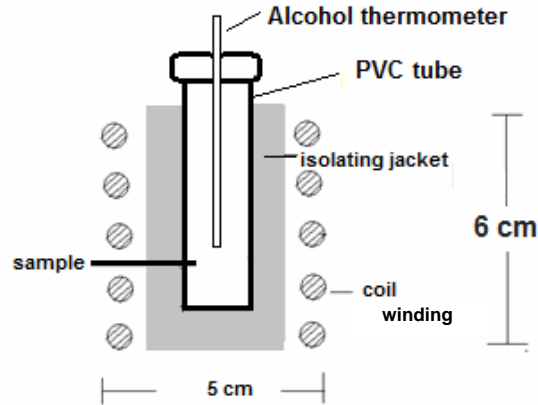
Fig. 1. Exposure set up of (CFC) to AMF using the induction heater. The alcohol thermometer, sample holder, insolating jacket and coil dimensions are shown.

CHEMOSENSITIVITY OF NANOPARTICLES (CELL VIABILITY)

Cytotoxic effect of nanoparticles was assessed by observation of changes with respect to viable and nonviable tumor cell count. Cytotoxicity effects of the CFC (0.5 mg to 15 mg) on Ehrlich ascite carcinoma cells (EACs) were determined according to the method of El-Merzabani *et al.*, (1979) [7]. In order to detect the cytotoxicity of CFC nanoparticles, Ehrlich ascites were treated with CFC (0.5 mg to 15 mg/mL) with and without application of AMF. The EACs were obtained by needle aspiration of ascites fluid from the preinoculated mice under aseptic condition using an ultraviolet laminar air flow system. The percentages of non viable cells were determined by counting dead and viable EACs. To differentiate between dead and viable EAC cells, trypan blue stain was used. Then the percentages of viable cells (V_C) were calculated according to equation (3), where (*C*) is number of viable cells and (*T*) is total number of cells.

$$\%V_C = \frac{C}{T} \times 100 \tag{3}$$

RESULTS AND DISCUSSION

STRUCTURAL ANALYSIS

The powder XRD pattern of the uncoated $CoFe_2O_4$ sample (CF) is shown in Fig. 2a. According to ICDD 000030864 database, the pattern showed a single phase spinel crystal structure. The lattice parameter was determined to be 8.3554 Å and the crystallite size 13 ± 1 nm (Fig. 2b). TEM micrographs and electron

diffraction pattern (Fig. 2c) of sample (CFC) shows the particle morphology and reveals a high degree of crystallinity.

The particle size distribution is also shown in Fig. 2b and the count is fitted with a log-normal function [2]. The average particle size is 13.56 nm (σ = 0.14). It is observed that the crystallite size obtained from XRD analysis and the particle size obtained from TEM analysis are in the same order of magnitude.
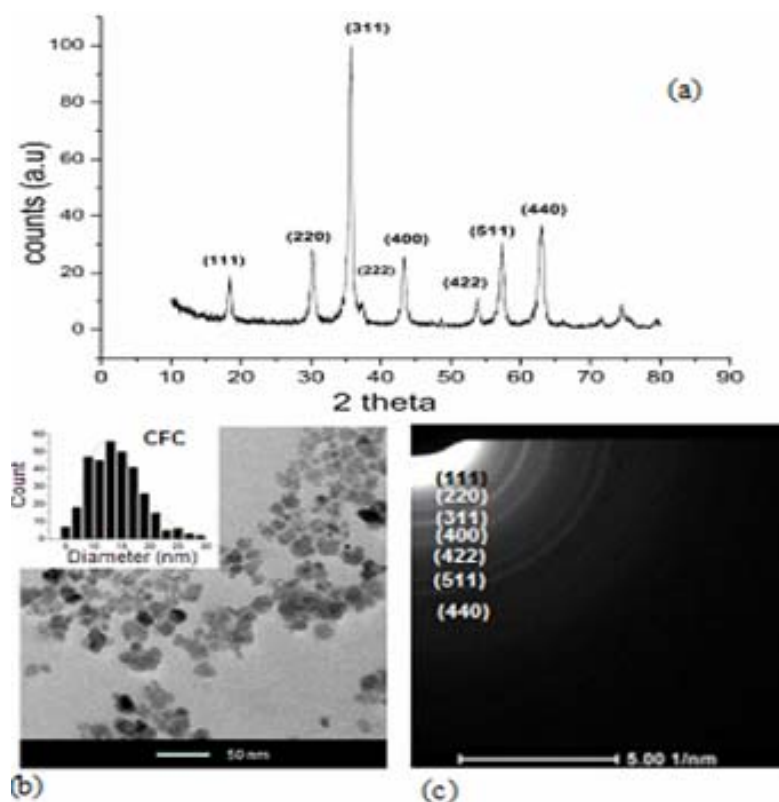

Fig. 2. a) X ray diffraction pattern for CF; b) TEM micrographs and lognormal distribution for CFC; c) selected area electron diffraction for CFC.

The binding of the biocompatible sodium citrate was denoted by the FTIR spectrum (Fig. 3). The spectrum reveals two bands around 410 and 600 cm^{-1} of the stretching vibration of (M–O) in the octahedral and tetrahedral sites in the cobalt ferrite respectively. The bands around 1600 and 3425 cm^{-1} represent the stretching vibration of O–H bond in the free or adsorbed water at the surface of the particles. The two bands around 1400 and 1600 cm^{-1} represent the asymmetric and symmetric stretching of C–O in COOH in (CFC) [10, 15, 27, 28, 29].
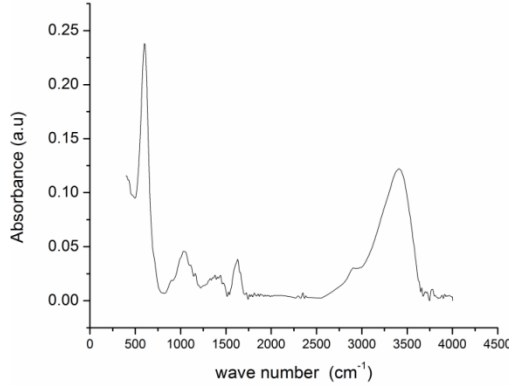
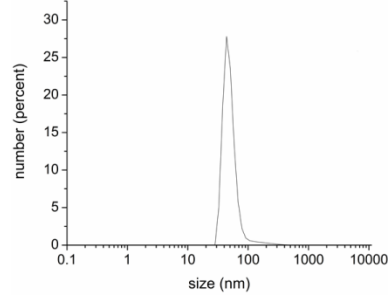Fig. 3. FTIR spectrum for sample CFC.

Fig. 4. Distribution of hydrodynamic size for CFC sample.

Zeta potential was utilized to confirm the citrate coating of cobalt ferrite. The citrate coated sample (CFC) has a zeta potential of –25.9 mV, and hydrodynamic size of 52 nm (Fig. 4). The observed negativity may be attributed to the hydroxyl groups on the surface of MNP in neutral pH, in addition to the free carboxylate groups from the sodium citrate coating [8]. This negativity is responsible for the colloidal stability maintained by electrostatic repulsion. Zeta potential of absolute value higher than 25 mV renders the particles electrostatically stable. The stability is further confirmed by the small hydrodynamic volume.

Generally, the absorption of the energy from the AMF and release of heat in the radiofrequency range is the basic idea of MFH. Rosensweig [36] developed a formula for the volumetric energy dissipation rate:

$$P = \mu_0 \pi \chi_0 f \frac{2\pi f \tau}{1 + (2\pi f \tau)} H^2$$

$$\tau = \frac{\tau_B \tau_N}{\tau_B + \tau_N}, \quad \tau_N = \tau_0 e^{\frac{KV_M}{k_B T}}, \quad \tau_B = \frac{3\eta V_H}{k_B T}$$

(4)

where μ_o is permeability of free space, f and H are the frequency and amplitude of the applied field respectively and χ_o is the initial (low field) DC magnetic susceptibility of the assembly of particles that depends on the physical and magnetic properties of the MNPs. This loss is due to relaxational losses with relaxation time τ. Relaxation losses fall into two categories, namely Brownian and Neel relaxations. Neel relaxation is the rotation of the magnetic moments inside the particle with a relaxation time τ_N. Brownian relaxation is the physical rotation of the particles against the viscosity barrier (magnetic moment locked along the easy direction of magnetization) with a relaxation time given by τ_B. The effective

relaxation time is τ [35, 41] where V_M is the volume of the magnetic core, $\tau_o \sim 10^{-9}-10^{-13}$ s [38], K is the effective anisotropy constant, k_B, T are the Boltzman constant and temperature in Kelvin respectively, η is the viscosity of the medium and V_H is the hydrodynamic volume of the particle. Equation (4) shows that the relaxation mechanism with the shorter time dominates. It is clear from equation (4) that increasing the field intensity H leads to increased heat dissipation. Nevertheless, H cannot be increased indefinitely to avoid violation of the safety guidelines.
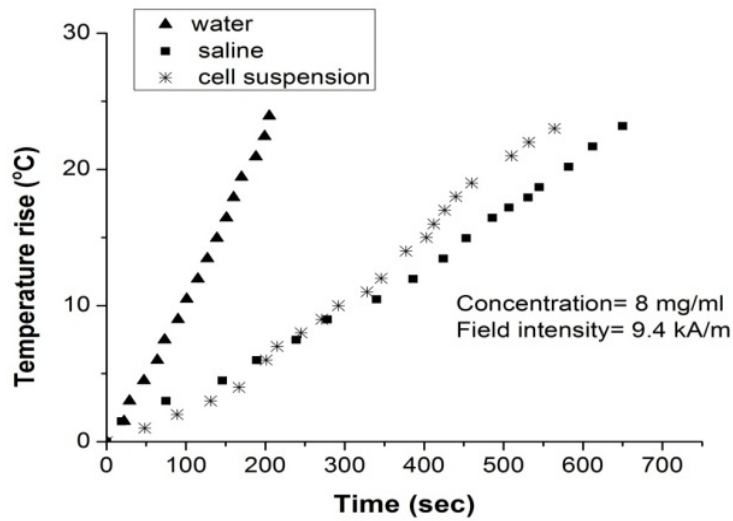

Fig. 5. Temperature rise with time for a concentration of 8 mg/mL at a field of 9.4 kA/m
with water and saline as solvents.

This section is concerned with the measurement of SAR for sample CFC. SAR measurement was carried out in a water based solution and in saline solution to determine the effect of the salt content in the biological media on the SAR values obtained from equation (2). Fig. 5 shows the temperature rise with time for sample CFC at a magnetic field intensity of 9414 (A/m), frequency of 198 kHz and sample concentration of 8 mg/mL. The obtained SAR value is 82.62 W/g. The dissipated heat is attributed to both Brownian and Neel loss mechanisms. It is necessary to determine the effect of the physiological conditions on the stability of the particles in solution and therefore on the contribution of the Brownian loss mechanism to the overall heat production.Fig. 5 also shows the temperature rise with time in case of saline and cell suspension. The rate of temperature rise ($\Delta T/t$) is reduced to less than one third of its value in case of saline as a solvent compared to water, giving a SAR of 22.3 W/g. The observed lowering of SAR values may be attributed to the salting out that causes sedimentation of the particles, thus decreasing the contribution of the Brownian loss mechanism [5]. Nevertheless, a

temperature of 47 °C which is suitable for thermoablation could be reached in 13 minutes. The results obtained in case of Ehrlich ascite cell suspension will be discussed shortly.

IN VITRO CYTOCOMPATIBILITY STUDY

In vitro cell viability essays used in this study do not provide information about the biodistribution of chemicals, their toxicity on the target organs or their metabolism and clearance. Nevertheless, this simple and fast test is carried out to estimate any possible death in the Ehrlich ascite carcinoma cells that may be "faultily" attributed to the hyperthermia treatment and thus, any correction terms can be considered. In addition, this easy assessment helps to determine the biocompatibility of the particles. This is throughly studying the effect of the actual biological media on the dispersion of the particles, which has a direct impact on the temperature profile of the magnetic fluid (MF). In this study, cell viability was calculated for the Ehrlich ascite carcinoma cells suspension after exposure to sample CFC at concentrations 0.5 to 15 mg/mL for two hours in an incubation temperature of 37 °C as shown in Fig. 7.
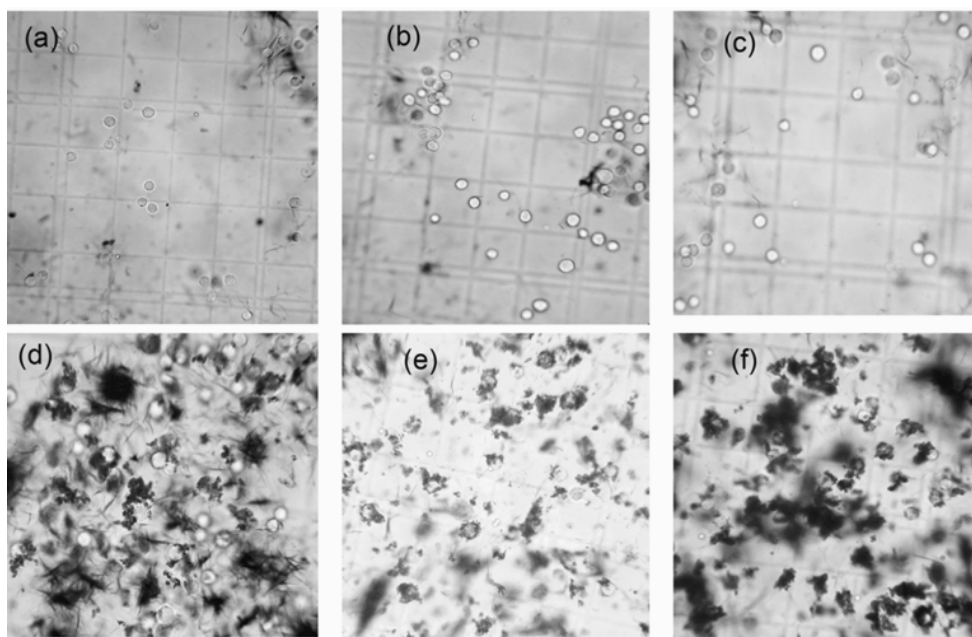

Fig. 6. Photomicrograph of Ehrlich ascite carcinoma cells under light microscope (400x) for Ehrlich ascites cells incubated for 2h with different concentration (mg/mL) of $CoFe_2O_{4\,a}$) 0.5, b)1.25, c) 2.5, d) 5, e) 10, and f) 15.
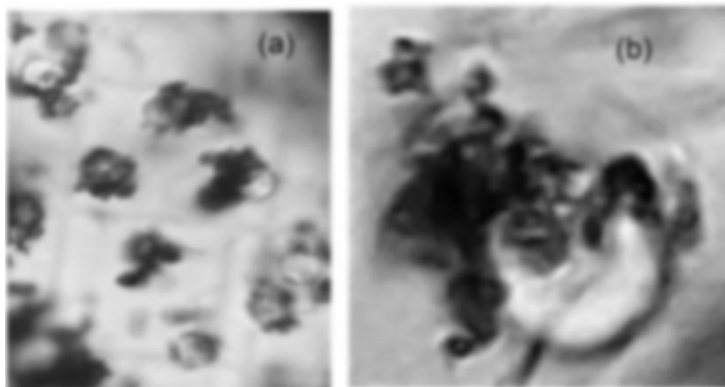
Fig. 7. a) Photomicrograph of Ehrlich ascite carcinoma cells show the nanoparticles adhesion
to tumor cell membrane for a concentration of 15 mg/mL of $CoFe_2O_4$.
b) High magnification of Ehrlich tumor cell using light microscope.

Cell death is not observed in the photomicrographs in Fig. 7, even at the highest concentration (15 mg/mL) for this short exposure duration. Cell counts (not shown here) show that the cell viability for all concentrations for a 2 hour incubation exceeded 98 %. It can thus be inferred that the short term exposure to the particles does not cause any considerable loss in the population of the cells. This implies that no correction terms need to be calculated for the assessment of cell viability after any hyperthermia treatment. Furthermore, the photomicrographs taken (Fig. 7) show that on increasing the concentration of the particles in the cell suspension from 0.5 to 15 mg /mL MNPs are agglomerated as expected due to the presence of opsonins [32] in the medium (in addition to the previously mentioned effect of salt content). The agglomeration of MNPs becomes more pronounced at high concentrations (5 mg/mL and higher). It is important to notice that the observed blue spots are merely caused by patches of trypan blue dye; this is independent of the concentration of CFC. Another important finding is that adhesion of the MNPs to the membrane is revealed by light microscope (Fig. 7). This adhesion may be attributed to the presence of cationic sites in the overall negatively charged cell membranes that nonspecifically bind the negatively charged MNPs. Such adhesion may lead to the internalization of the particles via endocytosis [39]. Massive endocytosis of cobalt ferrite MF was observed in mammary tumors after 20 min of inoculation [37]. An earlier study [20] on 8.2 nm citrate-coated cobalt ferrite-based MF revealed that the citrate coating layer was damaged and the NMPs agglomerated but still the study considered it as biocompatible.

IN VITRO HYPERTHERMIA

The target of the study is to entirely kill cancer cells and reach a viability of zero. The challenge is to achieve the mentioned goal with minimum concentration of CFC as a priority and without violating the proposed safety guidelines. *In vitro* hyperthermia is a simple set up that gives insight about the efficiency of the MNPs in hyperthermia and has been previously used [18]. The therapeutic conditions will be optimized if the total exposure time of the AMF application is also minimized. The two selected temperatures are 47 and 57 °C. The first therapeutic temperature was achieved by two concentrations of CFC: 5.29 and 8 mg/mL of cell suspension. The second temperature was achieved only by a concentration of 8 mg/mL. The applied field was manually controlled such that the temperature was rapidly raised to the desired temperature and held constant to durations up to 60 minutes. The maximum field intensity used in this study is 9.4 kA/m, therefore the product of the applied field and frequency did not exceed the proposed safety limits.

Referring to Fig. 5, a slight enhancement in SAR value is observed in cell suspension (29.8 W/g) compared to saline (23.3 W/g). Further drop in SAR values was expected in biological media which contain opsonins that may further lead to particle agglomeration in addition to the presence of cell membranes which may further hinder the Brownian rotation of the particles. On the other hand, cell membranes may provide large surface area that helps in dispersing the particles which leads to a more homogeneous temperature distribution in the sample. This factor may be responsible for the observed slight increase in SAR values.

Each exposure set-up was repeated three times the cell viability was calculated from equation (3). Fig. 8 shows the cell viability for the different exposure set-ups.
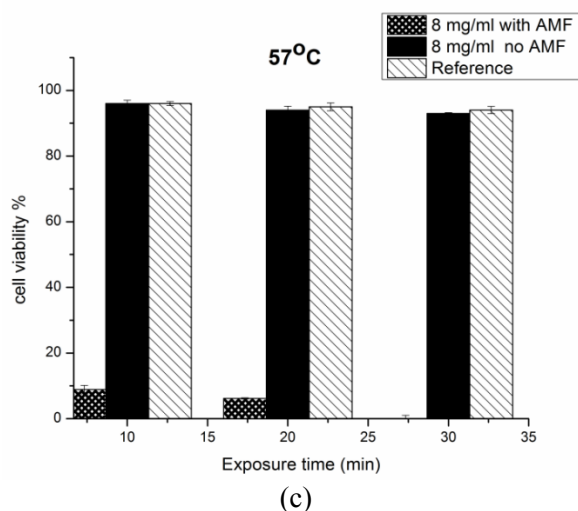

(a)   (b)

(c)
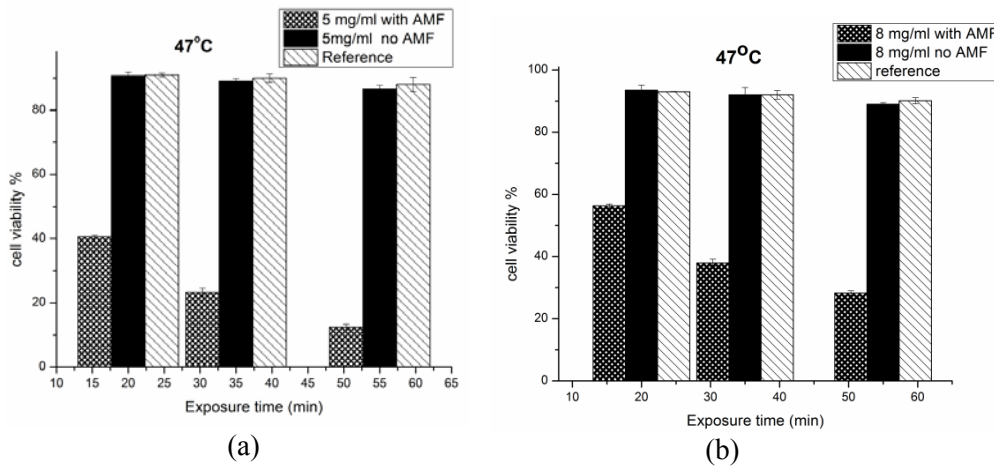
Fig. 8. Cell viability of Ehrlih ascites cells for different exposure set-ups. a) and b) therapy at 47 ^{o}C using 5 and 8 mg/mL, respectively, c) therapy at 57 ^{o}C using 8 mg/mL.

Comparing the cell viability after 60 minutes for the two exposure conditions at 47 °C, namely using 5 and 8 mg/mL, shows that a better efficiency is achieved at the low concentration. This can be understood by referring to Fig. 7. The figure shows the adherence of the particles to the cell membrane resulting in the conduction of heat from the particles to the membrane directly in addition to heat dissipation to the surrounding fluid. Further increment of particle concentration above a certain value leads to further agglomeration of the particles to the membrane thus insulating it from the surrounding environment. These excess particles ultimately cause a false temperature measurement in which the temperature of the fluid is higher than that of the cells. In the third exposure case at 57 °C, this very high temperature (even if higher than the actual temperature of the cells) is sufficient to cause the viability to drop to zero after a 30 min exposure.

CONCLUSIONS

In this study a stable colloid based on cobalt ferrite MNP has been prepared. The sample has a particle size of 13.56 ($\sigma = 0.14$).

A SAR value of 82.6 W/g was obtained at a frequency of 198 kHz and a magnetic field intensity 9.4 kA/m in water based colloid. A lowering in SAR values (20.2 W/g) is observed in saline based colloids due to particle agglomeration.

Cytotoxicity assessments depicted no considerable decrease in the cell viability as a result of short term exposure to cobalt ferrite concentrations up to 15 mg/mL. Therefore, no correction terms need to be considered.

In vitro hyperthermia led to a very important result; there exists an optimum concentration of the citrate coated cobalt ferrite particles that achieves the desired temperature profile at a certain field. Further increase in the concentration leads to faulty temperature measurements and thus decreased efficiency due to excessive toxicity.

Complete cell death was achieved at a therapeutic temperature of 57 °C for 30 minutes at a concentration of 8 mg/mL without violating the safety limits.

The authors consider cobalt ferrite a promising candidate for MFH and future work will be devoted for enhancing its properties.

REFERENCES

1. AYYAPPAN, S., S. MAHADEVAN, P. CHANDRAMOHAN, M.P. SRINIVASAN, J. PHILIP, B. RAJ, Influence of Co^{2+} ion concentration on the size, magnetic properties, and purity of $CoFe_2O_4$ spinel ferrite nanoparticles, *J. Phys. Chem. C*., 2010, **114**(14), 6334–6341.

2. BABIĆ-STOJIĆ, B., V. JOKANOVIĆ, D. MILIVOJEVIĆ, Z. JAGLIČIĆ, D. MAKOVEC, N. JOVIĆ, *et al*., Magnetic and structural studies of $CoFe_2O_4$ nanoparticles suspended in an organic liquid, *J. Nanomater.*, 2013, 741036, 9 pp.

3. BALDI, G., D. BONACCHI, M.C. FRANCHINI, D. GENTILI, G. LORENZI, A. RICCI, *et al.*, Synthesis and coating of cobalt ferrite nanoparticles: a first step toward the obtainment of new magnetic nanocarriers, *Langmuir*., 2007, **23**(7), 4026–4028.

4. BISWAL, D., B.N. PEEPLES, C. PEEPLES, A.K. PRADHAN, Tuning of magnetic properties in cobalt ferrite by varying Fe^{+2} and Co^{+2} molar ratios, *J. Magn. Magn. Mater.*, 2013, **345**, 1–6.

5. CHEN, S, C. CHIANG, S. HSIEH, Simulating physiological conditions to evaluate nanoparticles for magnetic fluid hyperthermia (MFH) therapy applications, *J. Magn. Magn. Mater.*, 2010, **322**(2), 247–252.

6. DEATSCH, A.E, B.A. EVANS, Heating efficiency in magnetic nanoparticle hyperthermia, *J. Magn. Magn. Mater.*, 2014, **354**, 163–172.

7. EL-MERZABANI, M.M., A.A. EL-AASER, M.A. ATTIA, A. K. EL DUWEINI, A. M. GHAZAL, Screening system for Egyptian plants with potential anti-tumor activity, *Planta Med*., 1979, **36**, 150–155.

8. FORTIN, J.-P., F. GAZEAU, C. WILHELM, Intracellular heating of living cells through Néel relaxation of magnetic nanoparticles, *Eur. Biophys. J.*, 2008, **37**(2), 223–228.

9. FRIMPONG, R.A., J. DOU, M. PECHAN, J.Z. HILT, Enhancing remote controlled heating characteristics in hydrophilic magnetite nanoparticles via facile co-precipitation, *J. Magn. Magn. Mater.*, 2010, **322**(3), 326–331.

10. GAO, H., G. WANG, M. YANG, L. TAN, J. YU, Novel tunable hierarchical Ni–Co hydroxide and oxide assembled from two-wheeled units, *Nanotechnology.*, 2012, **23**(1), 15607, 8 pp.

11. GILCHRIST, R.K, R. MEDAL, W.D. SHOREY, R.C. HANSELMAN, J.C. PARROTT, C.B. TAYLOR, Selective inductive heating of lymph nodes, *Ann. Surg.*, 1957, **146**(4), 596–606.

12. HERGT, R., S. DUTZ, Magnetic particle hyperthermia – biophysical limitations of a visionary tumour therapy, *J. Magn. Magn. Mater.*, 2007, **311**(1), 187–192.

13. HERMAN, T.S, B.A. TEICHER, M. JOCHELSON, J. CLARK, G. SVENSSON, C.N. COLEMAN, Rationale for use of local hyperthermia with radiation therapy and selected anticancer drugs in locally advanced human malignancies, *Int. J. Hyperth.*, 1988, **4**(2), 143–158.

14. HO, D., X. SUN, S. SUN, Monodisperse magnetic nanoparticles for theranostic applications, *Acc. Chem. Res.*, 2011, **44**(10), 875–882.

15. HOU, R., G. ZHANG, G. DU, D. ZHAN, Y. CONG, Y. CHENG, *et al.*, Colloids and surfaces B: Biointerfaces magnetic nanohydroxyapatite / PVA composite hydrogels for promoted osteoblast adhesion and proliferation, *Colloids Surfaces B Biointerfaces*, 2013, **103**, 318–325.

16. HUANG, S., S.Y. WANG, A. GUPTA, D.A. BORCA-TASCIUC, S.J. SALON. On the measurement technique for specific absorption rate of nanoparticles in an alternating electromagnetic field, *Meas. Sci. Technol.*, 2012, **23**(3), 35701, 6 pp.

17. JIAN, L., Y. SHI, J. LIANG, C. LIU, G. XU, A novel targeted magnetic fluid hyperthermia system using HTS coil array for tumor treatment, *Appl. Supercond. IEEE Trans.*, 2013, **23**(3), 4400104, 4pp.

18. KHANDHAR, A.P., R.M. FERGUSON, J.A. SIMON, K.M. KRISHNAN, Enhancing cancer therapeutics using size-optimized magnetic fluid hyperthermia, *J. Appl. Phys.*, 2012, **111**(7), 07B306, 3pp.

19. KOZISSNIK, B., A.C. BOHORQUEZ, J. DOBSON, C. RINALDI, Magnetic fluid hyperthermia: Advances, challenges, and opportunity, *Int. J. Hyperth.*, 2013, **29**(8), 706–714.

20. KÜCKELHAUS, S., V.A.P. GARCIA., L.M. LACAVA, R.B. AZEVEDO, Z.G.M. LACAVA, E.C.D. LIMA *et al.*, Biological investigation of a citrate-coated cobalt–ferrite-based magnetic fluid, *J. Appl. Phys.*, 2003, **93**(10), 6707–6708.

21. KÜCKELHAUS, S., S.C. REIS, M.F.CARNEIRO, A.C. TEDESCO, D.M. OLIVEIRA, E.C.D. LIMA, *et al.*, *In vivo* investigation of cobalt ferrite-based magnetic fluid and magnetoliposomes using morphological tests, *J. Magn. Magn. Mater.*, 2004, **272**, 2402–2403.

22. KUMAR, C.S.S.R, F. MOHAMMAD, Magnetic nanomaterials for hyperthermia-based therapy and controlled drug delivery, *Adv. Drug Deliv. Rev.*, 2011, **63**(9), 789–808.

23. LUTTEROTTI, L., MAUD materials analysis using diffraction version 2.33, 2011, http//www ing unitn it/~ maud.

24. MA, M., Y. WU, J. ZHOU, Y. SUN, Y. ZHANG, N. GU, Size dependence of specific power absorption of Fe3O4 particles in AC magnetic field, *J. Magn. Magn. Mater.*, 2004, **268**(1), 33–39.

25. MAAZ, K., A. MUMTAZ, S.K. HASANAIN, A. CEYLAN, Synthesis and magnetic properties of cobalt ferrite ($CoFe_2O_4$) nanoparticles prepared by wet chemical route, *J. Magn. Magn. Mater.*, 2007, **308**(2), 289–295.

26. MASSART, R., E. DUBOIS, V. CABUIL, E. HASMONAY, Preparation and properties of monodisperse magnetic fluids, *J. Magn. Magn. Mater.*, 1995, **149**(1), 1–5.

27. MOHAPATRA. J, A. MITRA, D. BAHADUR, M. ASLAM, Surface controlled synthesis of MFe_2O_4 (M = Mn, Fe, Co, Ni and Zn) nanoparticles and their magnetic characteristics, *Cryst. Eng. Comm.*, 2013, **15** (3), 524–532.

28. MOJIĆ, B., K.P. GIANNAKOPOULOS, Ž. CVEJIĆ, V.V. SRDIĆ, Silica coated ferrite nanoparticles: Influence of citrate functionalization procedure on final particle morphology, *Ceram. Int.*, 2012, **38**(8), 6635–66341.

29. MORAIS, P.C, R.L. SANTOS, A.C.M. PIMENTA, R.B. AZEVEDO, E.C.D. LIMA, Preparation and characterization of ultra-stable biocompatible magnetic fluids using citrate-coated cobalt ferrite nanoparticles, *Thin Solid Films*, 2006, **515**(1), 266–270.

30. MORNET, S., S. VASSEUR, F. GRASSET, E. DUGUET, Magnetic nanoparticle design for medical diagnosis and therapy, *Journal of Materials Chemistry.*, 2004, **14**, 2161–2175.
31. MOZAFFARI, M., S. MANOUCHEHRI, M.H .YOUSEFI, J. AMIGHIAN, The effect of solution temperature on crystallite size and magnetic properties of Zn substituted Co ferrite nanoparticles, *J. Magn. Magn. Mater*., 2010, **322**(4), 383–388.
32. NAGAYAMA, S., K. OGAWARA, Y. FUKUOKA, K. HIGAKI, T. KIMURA, Time-dependent changes in opsonin amount associated on nanoparticles alter their hepatic uptake characteristics, *Int. J. Pharm.,* 2007, **342**(1), 215–221.
33. OVERGAARD, J., D. GONZALEZ, M. HULSHOF, G. ARCANGELI, O. DAHL, O. MELLA, *et al.*, Hyperthermia as an adjuvant to radiation therapy of recurrent or metastatic malignant melanoma. A multicentre randomized trial by the European Society for Hyperthermic Oncology, *Int. J. Hyperth*., 2009, **25**(5), 323–334.
34. RASHIN, M.N., J. HEMALATHA, Magnetic and ultrasonic studies on stable cobalt ferrite magnetic nanofluid, *Ultrasonics,* 2014, **54** (3), 834–840.
35. RONDINONE, A.J, A.C.S. SAMIA, Z.J. ZHANG, Characterizing the magnetic anisotropy constant of spinel cobalt ferrite nanoparticles, *Appl. Phys. Lett*., 2000, **76**(24), 3624–3626.
36. ROSENSWEIG, R.E., Heating magnetic fluid with alternating magnetic field, *J. Magn. Magn. Mater*., 2002, **252**, 370–374.
37. ŞINCAI, M., D. GÂNGĂ, D. BICA, L.VÉKÁS, The antitumor effect of locoregional magnetic cobalt ferrite in dog mammary adenocarcinoma, *J. Magn. Magn. Mater*., 2001, **225**(1), 235–240.
38. TUNG, L.D., V. KOLESNICHENKO, D. CARUNTU, N.H. CHOU, C.J. O'CONNOR, L. SPINU, Magnetic properties of ultrafine cobalt ferrite particles, *Journal of Applied Physics,* 2003, **93,** 7486–7488.
39. VERMA, A., F. STELLACCI, Effect of surface properties on nanoparticle-cell interactions, *Small*., 2010, **6**(1), 12–21.
40. WANG, Y.M., X. CAO, G.H. LIU, R.Y. HONG, Y.M. CHEN, X.F. CHEN, *et al.*, Synthesis of Fe_3O_4 magnetic fluid used for magnetic resonance imaging and hyperthermia, *J. Magn. Magn. Mater*., 2011, **323**(23), 2953–2959.
41. ZHANG, L.Y, H.C. GU, X.M. WANG, Magnetite ferrofluid with high specific absorption rate for application in hyperthermia, *J. Magn. Magn. Mater*., 2007, **311**(1), 228–233.
42. ZHAO, L., B. YANG, J. TANG, M. HUO, X. WANG, X. XU, *et al.*, Magnetic nanocomposite devices for cancer thermochemotherapy, *INTECH Open Access Publisher*., 2011, pp. 386–402.